Aerosol Science and Technology

ISSN: (Print) (Online) Journal homepage: https://www.tandfonline.com/loi/uast20

Emissions and radiative impacts of sub-10 nm particles from biofuel and fossil fuel cookstoves

Shantanu H. Jathar , Naman Sharma , Kelsey R. Bilsback , Jeffrey R. Pierce , Joonas Vanhanen , Timothy D. Gordon & John Volckens

To cite this article: Shantanu H. Jathar , Naman Sharma , Kelsey R. Bilsback , Jeffrey R. Pierce , Joonas Vanhanen , Timothy D. Gordon & John Volckens (2020) Emissions and radiative impacts of sub-10 nm particles from biofuel and fossil fuel cookstoves, Aerosol Science and Technology, 54:10, 1231-1243, DOI: 10.1080/02786826.2020.1769837

To link to this article: https://doi.org/10.1080/02786826.2020.1769837

AEROSOL SCIENCE AND TECHNOLOGY
2020, VOL. 54, NO. 10, 1231–1243
https://doi.org/10.1080/02786826.2020.1769837

Emissions and radiative impacts of sub-10 nm particles from biofuel and fossil fuel cookstoves

Shantanu H. Jathar[a], Naman Sharma[a], Kelsey R. Bilsback[b], Jeffrey R. Pierce[b], Joonas Vanhanen[c], Timothy D. Gordon[d], and John Volckens[a]

[a]Mechanical Engineering, Colorado State University, Fort Collins, Colorado, USA; [b]Atmospheric Science, Colorado State University, Fort Collins, Colorado, USA; [c]Airmodus Ltd, Helsinki, Finland; [d]Handix Scientific, Boulder, Colorado, USA

ABSTRACT

Combustion sources have been shown to directly emit particles smaller than 10 nm. The emission of 1-3 nm particles from biofuel or fossil fuel cookstoves has not been studied previously, nor have the radiative impacts of these emissions been investigated. In this work, emissions (number of particles) were measured during a water boiling test performed on five different cookstoves (three-stone fire, rocket elbow, gasifier, charcoal, and liquified petroleum gas [LPG]) for particle diameters between ~1 and ~1000 nm. We found significant emissions of particles smaller than 10 nm for all cookstoves ($>5 \times 10^{15}$ # kg-fuel^{-1}). Furthermore, cleaner (e.g., LPG) cookstoves emitted a larger fraction of sub-10 nm particles (relative to the total particle counts) than traditional cookstoves (e.g., three-stone fire). Simulations performed with the global chemical transport model GEOS-Chem-TOMAS that were informed by emissions data from this work suggested that sub-10 nm particles were unlikely to significantly influence number concentrations of particles with diameters larger than 80 nm that can serve as cloud condensation nuclei (CCN) (<0.3%, globally averaged) or alter the cloud-albedo indirect effect (absolute value <0.005 W m^{-2}, globally averaged). The largest, but still relatively minor, localized changes in CCN-relevant concentrations (<10%) and the cloud-albedo indirect effect (absolute value <0.5 W m^{-2}) were found in large biofuel combustion source regions (e.g., Brazil, Tanzania, Southeast Asia) and in the Southern Ocean. Enhanced coagulation-related losses of these sub-10 nm particles at subgrid scales will tend to further reduce their impact on particle number concentrations and the aerosol indirect effect, although they might still be of relevance for human health.

ARTICLE HISTORY
Received 15 April 2020
Accepted 8 May 2020

EDITOR
Nicole Riemer

1. Introduction

Direct emissions from natural and anthropogenic combustion are an important source of sub-micron particles to the atmosphere. These emissions contribute substantially to the atmospheric aerosol burden and subsequently have large impacts on climate (Pachauri et al. 2014) and human health (Apte et al. 2015). Yet the sources, formation pathways, properties, and atmospheric impacts of combustion-related aerosol remain active areas of research (Fuzzi et al. 2015).

Numerous studies have measured number emissions of ultrafine particles (10-100 nm) from combustion sources (Huang et al. (2013) (gasoline vehicles) Herner et al. (2011) (diesel vehicles); Just, Rogak, and Kandlikar (2013) and Tryner, Volckens, and Marchese (2018) (cookstoves)) but few have measured those for particles sizes smaller than 5 nm. Recently, a handful of studies have leveraged new instrumentation (e.g., A11 nCNC by Airmodus Ltd. (Kangasluoma et al. 2016), 1-nm SMPS by TSI Inc. (Stolzenburg et al. 2018)) to study the particle size distribution below 5 nm from combustion sources in laboratory and near-road environments. Alanen et al. (2015) and Rönkkö et al. (2017) measured particle emissions from a natural gas and diesel engine respectively while Järvinen et al. (2019) measured the same from a fleet of public diesel buses. Particle emissions for diameters larger than ~1 nm from these sources ranged from 10^{12} # kg-fuel^{-1} to larger than 10^{15} # kg-fuel^{-1} and, in most instances, the overall number emissions were dominated (>50%) by particle diameters below 3 nm.

CONTACT Shantanu H. Jathar shantanu.jathar@colostate.edu Mechanical Engineering, Colorado State University, 200 W. Lake St., 1374 Campus Delivery, Fort Collins, CO 80523, USA.

Supplemental data for this article is available online at https://doi.org/10.1080/02786826.2020.1769837.

Rönkkö et al. (2017) and Hietikko et al. (2018) measured ambient concentrations at a near-road site and in a street canyon respectively and estimated the traffic-related sub-3 nm particle emissions to exceed 10^{15} # kg-fuel^{-1}. While these sub-5 nm particles have been measured for fossil-fuel engines, these emissions have not been studied for other combustion sources. Biomass combustion – broadly defined here as including residential wood combustion, prescribed burning, and wildfires – is a dominant source of sub-micron particle mass and number to the atmosphere (Granier et al. 2011), and hence it is vital that we also study sub-5 nm particle emissions from this source category.

Primary emissions of particles from combustion sources, rather than particles formed via nucleation, are the dominant source of cloud condensation nuclei (CCN) in many parts of the atmosphere and strongly influence aerosol-cloud interactions (Ramnarine et al. 2019; Gordon et al. 2017; Kodros et al. 2015, 2016; Spracklen et al. 2007). Studies that have measured sub-5 nm particle emissions from combustion sources have argued that emissions of these particles could be sufficient to alter CCN concentrations and impact the radiative balance through the aerosol indirect effect (Rönkkö et al. 2017). Particles smaller than 10 nm collide and coagulate rapidly with larger particles and have relatively short lifetimes in the atmosphere (<1 h) (Hinds 2012). While only a few can survive long enough to grow and serve as CCN (Westervelt et al. 2013; Kuang, McMurry, and McCormick 2009), the ability of sub-5 nm particle emissions to influence CCN-relevant concentrations will depend on background and in-plume aerosol concentrations, mixing ratios and volatility of condensable vapors, and ambient conditions (Stevens et al. 2012; Pierce et al. 2011; Kerminen and Wexler 1996). Direct emissions of sub-5 nm particles are typically not accounted for in large-scale atmospheric models and hence their impacts on the aerosol indirect effect remain uncertain.

In this work, we measured combustion emissions of particles ranging in size from ~1 to ~1000 nm from a cross-section of biofuel and fossil fuel cookstoves. The cookstoves were chosen to represent the transition in an energy ladder from traditional (e.g., three-stone fire) to fossil fuel cookstoves (e.g., liquified petroleum gas). Our emissions measurements were incorporated in simulations with a global chemical transport model to predict changes in the particle number concentrations and the cloud-albedo indirect effect from the addition of a sub-10 nm particle mode.

2. Methods

2.1. Cookstove emissions experiments and analysis

We performed seven experiments with five different cookstoves in the Colorado State University (CSU) emissions hood. A schematic of the experimental setup is shown in Figure S1. The emissions hood, previously described in Tryner et al. (2016), consists of an acrylic enclosure built on an aluminum frame ($1.2 \times 1.2 \times 4.3$ m) that is large enough to hold a cookstove and a pot on the ground. The top of the acrylic enclosure is connected to a conical aluminum section that feeds to an aluminum duct (12.7 cm OD). A constant-volume displacement pump at the end of the duct is used to pull laboratory air through the emissions hood at a flow rate of 0.1 m^3 s^{-1} (6000 L min^{-1}). This flow rate is similar to average flow rates calculated from kitchen volumes (~30 m^3) and air changes per hour (~15) observed with cookstove use in developing countries (Raiyani et al. 1993; Albalak et al. 2001; Park and Lee 2003; Clark et al. 2010). Average residence times for emissions within the hood are on the order of one minute.

The following five cookstoves were used in this study: (i) three-stone fire, (ii) rocket elbow (G-3300; Envirofit Inc.), (iii) gasifier (ACE/1; African Clean Energy), (iv) charcoal jiko (artisan made), and (v) liquefied petroleum gas (LPG) (WD-C1-25k; WokSmith Inc.). The cookstoves were chosen based on the work of Bilsback et al. (2019) who measured and analyzed primary emissions from a combination of eleven different cookstoves and ten different fuels. The cookstoves in this study, from the three-stone fire to the LPG, roughly spanned the range from low to high, respectively, of particulate matter (PM) mass emissions measured by Bilsback et al. (2019). We used Douglas fir cut into $5 \times 2.5 \times 20$ cm stock as fuel for the three-stone fire and rocket elbow stoves and Douglas fir chipped into pellets (~5 cm) as fuel for the gasifier stove. Hardwood lumps were used as fuel for the charcoal stove, and propane gas was used as fuel for the LPG stove. The Douglas fir, hardwood lumps, and propane gas were all sourced locally.

A single test was performed for the five cookstoves in 2018 and two repeats were performed for the rocket elbow and LPG cookstoves in 2020. Details of the cookstove experiments are provided in Table S1. The duct blower was run for at least 15 min before starting the cookstove and this period was used to determine background particle levels with the A11 and SMPS. During this time the unignited cookstove

and a pot with 5 kg of tap water were placed in the hood. We performed an approximate version of the water boiling test (WBT 2014) with each cookstove that included the following: (i) a 'cold start' where 5 kg of tap water was heated to 90 °C at maximum firepower, (ii) a 'hot start' immediately after the cold start where 5 kg of tap water was heated to 90 °C at maximum firepower, and (iii) a 'simmer' following the hot start where the stove firepower was adjusted to hold the water near 90 °C (±6 °C) for 45 min. We did not follow the WBT protocol exactly since our focus was not on conducting a performance test (Jetter et al. 2012). Except for the LPG that used an electric igniter, we used a small amount of lighter fluid to ignite the fuel for the solid fuel cookstoves. The emissions data were filtered to exclude ignition events. The cookstoves were not reignited between the cold and hot and hot and simmer phases.

Emissions from the hood were sampled through two inlets held in line to the flow in the duct and located approximately 4 m above the stove pot. One of the inlet lines (0.6 cm ID, 51 cm long) was connected to an A11 nCNC system (Airmodus Ltd., Finland; 2.5 L min^{-1}) that consisted of a particle size magnifier (A10 PSM) and a condensation particle counter (A20 CPC). The A11 measures the particle number size distribution between the sizes of 1.3 and 3.3 nm and also provides a total number measurement for particle sizes between 3.3 and 1000 nm. The sample leading to the A11 had to be diluted to ensure that the particle concentrations were below the instrument's saturation limit (<100,000 cm^{-3}). The dilution was performed by mixing particle-free air, controlled using a mass flow controller, with the sample flow using a Swagelok 'tee'. We used a dilution ratio of ~100 for the solid fuel cookstoves and a dilution ratio of ~10 for the LPG. The other inlet line (0.6 cm ID, ~100 cm long) was connected to a scanning mobility particle sizer (SMPS; GRIMM Aerosol Technik, Germany; 0.3 L min^{-1}) to measure the particle size distribution between 11 and 1116 nm (or 5 to 350 nm) and a non-dispersive infrared gas analyzer (LI-840A; LI-COR Biosciences, Nebraska; 1 L min^{-1}) to measure mixing ratios of CO_2. By diluting primary emissions in the hood, the saturation limits were not exceeded on either instrument (<10^7 cm^{-3} for the SMPS while scanning and <10,000 ppm for the LI-840A). Another LI-840A was used to sample background CO_2 concentrations in the incoming dilution air near the opening at the bottom of the emissions hood.

Raw particle number concentrations from the A11 were processed using a custom Scilab code from Airmodus Ltd. to correct for coincidence errors and for diffusion losses in the A11 (Carnerero et al. 2018); the code can be found at https://github.com/Airmodus/A11_Scan. The particle number concentrations were additionally corrected for transmission losses in the sampling line (0.6 cm ID, ~50 cm long) using a custom IGOR code from von der Weiden et al. (2009), noting that most of the losses in this line were from particle diffusion. Corrections were also performed for the SMPS data but the transmission losses in this line (0.6 cm ID, ~100 cm long) were found to be much smaller than those in the sampling line for the A11. Both A11 and SMPS data were corrected for background concentrations measured prior to the start of the experiment. Size-resolved particle number concentrations ($dn\ dlogdp^{-1}$ in cm^{-3}) and total particle number concentrations (N_{total} in cm^{-3}) were converted to an emission factor basis using the following equation:

$$EF_X = \frac{\Delta X}{\Delta CO_2} \times \frac{MW_{CO_2}}{AW_C} \times C_f \times 10^{15} \quad - \qquad (1)$$

where ΔX is the background-corrected particle number concentration ($dn\ dlogdp^{-1}$ or N_{total}) in cm^{-3}, ΔCO_2 is the background-corrected CO_2 concentration in μg m^{-3}, MW_{CO_2}(44 g $mole^{-1}$) and AW_C (12 g $mole^{-1}$) are the molecular/atomic weights for CO_2 and carbon, and C_f is the mass fraction of carbon in the fuel. We used a C_f of 0.49, 0.84, and 0.85 g kg-$fuel^{-1}$ for the Douglas fir, hardwood lumps, and LPG respectively (Bilsback et al. 2019). This formulation for the emission factor calculation assumes that all of the carbon in the fuel was released as CO_2. Since CO, volatile organic compounds, and PM emissions are expected to be less than 10% of the CO_2 emissions on a carbon mass basis (Ward 1990) and that the cookstove was operated at maximum firepower and a high modified combustion efficiency, the assumption of only using CO_2 to determine the emission factor introduced a less than 10% error in the emission factor calculation.

2.2. Global chemical transport modeling and analysis

We performed simulations with the GEOS-Chem-TOMAS chemical transport model (v12.6.0; http://www.geos-chem.org) to determine the influence of sub-10 nm particle emissions on particle number concentrations and the cloud-albedo indirect effect. Aerosols are modeled in GEOS-Chem using the TwO Moment Aerosol Sectional (TOMAS) scheme, which tracks the number and mass moments of the aerosol

size distribution (Pierce, Chen, and Adams 2007; Adams and Seinfeld 2002). TOMAS simulates the key aerosol processes of nucleation, coagulation, condensation, and evaporation. In TOMAS, the aerosol size distribution is represented using 15 size bins that range from 3 to 10,000 nm and include the following aerosol species: black carbon (BC), organic aerosol (OA), sulfate, sea salt, and dust (Lee and Feingold 2013). Details about the nucleation schemes (Westervelt et al. 2013; Jung et al. 2010), secondary organic aerosol formation (Pai et al., 2020; D'Andrea et al. 2013; Spracklen et al. 2011), and inorganic aerosol thermodynamics (Adams et al. 2001) can be found in earlier publications.

The model was run at 4°×5° with 47 vertical layers for the year 2016. Meteorological inputs came from the GEOS Forward Processing offline meteorological fields (GEOS-FP; https://gmao.gsfc.nasa.gov/). We used CEDS as the base anthropogenic emissions inventory (Hoesly et al. 2018) along with several regional inventory overwrites including: APEI over Canada; NEI2011 over the United States; DICE-Africa over Africa (Marais and Wiedinmyer 2016); and MIXv2010 over China and Asia (Li et al. 2017). Biomass burning emissions were from van der Werf et al. (2017) (GFED4). Sea salt and mineral dust aerosol emissions followed the Jaeglé et al. (2011) and Zender et al. (2003) schemes, respectively. Biogenic emissions were based on MEGAN v2.1 with updates from Guenther et al. (2012).

In the default version of GEOS-Chem-TOMAS, particles from all anthropogenic combustion sources (e.g., fossil fuels, biofuels) are emitted using a log-normal size distribution with a single mode. These particle emissions were initialized with a geometric mean (μ) of 60 nm and a geometric standard deviation (σ) of 3 based on fitting the median particle size distribution measured in this work for solid fuel cookstoves; this is hereafter referred to as the 'larger' mode. This configuration, which produced few particles below 10 nm, was used to perform a BASE simulation and this simulation served as a control. We should note that as GEOS-Chem-TOMAS groups emissions from all anthropogenic combustion sources together, we were unable to change the size distribution for biofuel use (e.g., cooking, heating) independently from the fossil fuel source. Two additional simulations were performed where we added a 'smaller' mode to represent the emissions of particles smaller than 10 nm. The number emissions for this smaller mode were assumed to be a factor of 1 and 10 of the total number emissions in the larger mode. These simulations were labeled SUB10_1× and SUB10_10× respectively. For both simulations, we assumed that the smaller mode had a μ of 1 nm and a σ of 2. As the smallest size bin in GEOS-Chem-TOMAS is 3 nm, the smaller mode was represented by distributing the number emissions in the size bins between 3 nm and 10,000 nm. In summary, we ensured that the integral of the number distribution of the smaller mode between the sizes of 3 and 10,000 nm was approximately a factor of 1 and 10 of the integral of the larger mode over the same size range. The rationale for the 1× and 10× scaling, values for the μ and σ, and the implications of only modeling particles sizes above 3 nm is discussed in Section 3.3. Three additional simulations ($BASE_{mod}$, $SUB10\_1\times_{mod}$, $SUB10\_10\times_{mod}$) were performed where particles from all anthropogenic combustion sources in the larger log-normal mode were initialized with a μ of 30 nm and σ of 2 (rather than a μ of 60 nm and σ of 3), which is the default configuration in GEOS-Chem-TOMAS (Pierce, Chen, and Adams 2007). These simulations were performed to examine the sensitivity in the model results to the use of a different particle size distribution. As the particle mass emissions were kept constant across all six simulations, in the three additional simulations, the use of a smaller μ resulted in higher number emissions for both the smaller and larger modes.

The cloud-albedo indirect effect was calculated following Kodros et al. (2016). First, the monthly averaged particle number and mass concentrations were used along with the activation parameterization of Abdul-Razzak and Ghan (2002) to calculate cloud droplet number concentrations (CDNCs). For this calculation, we assumed the aerosol species to be internally mixed within each particle size bin, the hygroscopicity parameter (κ) to be a volume-weighted average of the individual species (Petters and Kreidenweis 2007), and a constant updraft velocity of 0.5 m s^{-1}. Next, we calculated the effective cloud droplet radius by assuming that the value for the control simulation was 10 μm and then multiplied this value by the ratio of the CDNC with and without the smaller mode to the one-third power (Rap et al. 2013; Scott 1968). Finally, the assumed and calculated effective cloud droplet radii and monthly mean cloud fraction, temperature, pressure, and liquid water content from GEOS-FP were used with the Rapid Radiative Transfer Model for Global Climate Models (Iacono et al. 2008) to predict the change in the top-of-the-atmosphere radiative flux.

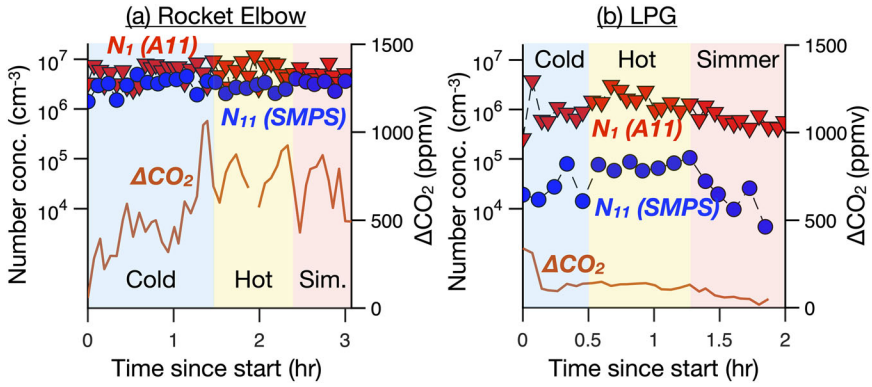

Figure 1. Background- and transmission-corrected particle number concentrations, N_1 and N_{11} in cm^{-3}, for the rocket elbow (a) and LPG (b) stoves during the experiments performed in 2018.

3. Results

3.1. Results from example experiments

We plot the time series for number concentrations and change in CO_2 mixing ratios from experiments performed on a rocket elbow and LPG in 2018 in Figure 1. N_1 and N_{11} refer to the number concentrations for particles larger than 1.1 and 11 nm as measured by the A11 and SMPS, respectively. Although we are actually calculating $N_{1.1}$, we round down $N_{1.1}$ to N_1 for simplicity and also to avoid confusion with N_{11}. All data presented in Figure 1 were corrected for background concentrations and transmission losses in the sampling line. We should note that the data in Figure 1 are concentrations and data normalized on a fuel-burned basis are presented in the subsequent sections. Being a relatively dirtier stove, the particle number concentrations from the rocket elbow were higher than those for the LPG; a factor of 5 larger for N_1 and two orders of magnitude larger for N_{11}. For both cookstoves, the N_1 emissions were larger than the N_{11} emissions although the N_1 emissions were more than an order of magnitude larger than the N_{11} emissions for the LPG. These results indicate substantial emissions of sub-10 nm particles for both cookstoves. Emissions from the rocket elbow did not seem to vary with the operating mode for the cookstove. For the LPG, the N_1 and N_{11} emissions seemed to reduce during the simmer phase, but this reduction might be linked to the lower firepower (and lower CO_2 emissions) required during the simmer test. The test performed on the rocket elbow and LPG were repeated in 2020 for N_{11} (but not for N_1) and, qualitatively, the N_{11} emissions were similar to those from tests performed in 2018 (Figure S2).

3.2. Particle number emission factors

The particle number emission factors, N_1 (panel a) and N_{11} (panel b), for the five different cookstoves are presented in Figure 2. The average and median N_{11} emissions varied between 4×10^{15} and 7×10^{15} kg-fuel^{-1} for the solid fuel cookstoves, but they were a factor of 5 to 10 smaller for the LPG (median of 8×10^{14} kg-fuel^{-1}). The emissions seemed to agree well with those measured from solid and gas fuel cookstoves in earlier studies (Bilsback et al. 2019; Shen et al. 2017) (see Table 1). The average and median N_1 emissions varied between 1×10^{16} to 4×10^{16} kg-fuel^{-1} for the five cookstoves, which suggested that, when compared to the N_{11} emissions, there were significant emissions of particles smaller than 11 nm. Unlike the N_{11} emissions, the LPG stove (median of $\sim 2 \times 10^{16}$ kg-fuel^{-1}) had similar N_1 emissions as the solid fuel cookstoves, and the charcoal cookstove was found to have twice the N_1 emissions (median of $\sim 4 \times 10^{16}$ kg-fuel^{-1}) than the others. Interestingly, the median fraction of the number emissions at particle diameters less than 11 nm seemed to steadily increase from ~43% for the traditional cookstove (three-stone fire) to 96% for the cleanest cookstove (LPG) (Figure 2c). This suggested that as the PM mass emissions are likely to reduce from the three-stone fire to the LPG cookstove, an increasing fraction of the particles were emitted at lower sizes. The N_1 and N_{11} emissions were not found to vary strongly with the operating mode (Figure S3). Average N_1 and N_{11} emission factors on a fuel burned basis as well as on an energy content basis (using the lower heating value of the fuel) are presented in Table S2.

The range of N_1 emissions from this work were compared against similar measurements performed for combustion sources in laboratory studies and in near-road environments (see Table 1). As mentioned earlier, the N_{11} emissions from this study ($1–7 \times 10^{15}$ kg-fuel^{-1}) were very similar to those measured by Shen et al. (2017) and Bilsback et al. (2019), but the N_1 emissions ($10–40 \times 10^{15}$ kg-fuel^{-1})

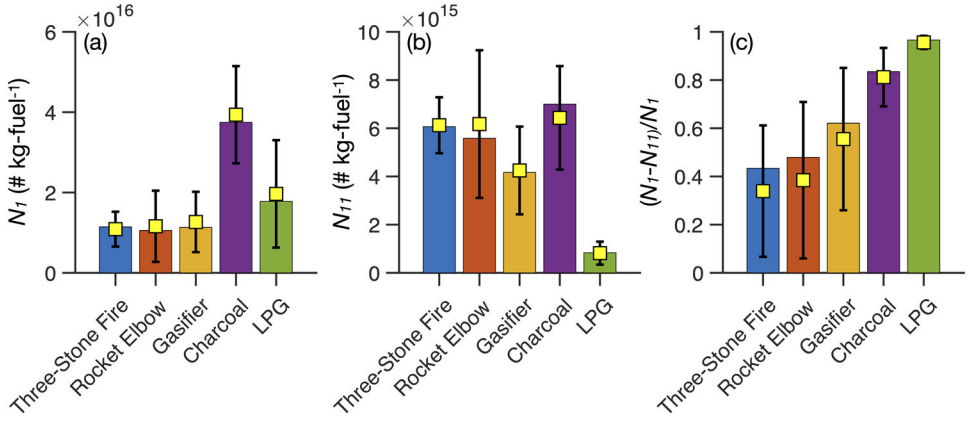

Figure 2. (a) Particle number emission factors (N_1) from the A11 measurements for particle sizes >1.1 nm and (b) particle number emission factors (N_{11}) from the SMPS measurements for particle sizes >11 nm. (c) Particle fraction of sub-11 nm particles. Y-axis limits in panels (a) and (b) are different. Bars represent medians while yellow squares and error bars represent the average value and one standard deviation, respectively.

Table 1. Particle number emission factors compared between this study and other laboratory and field studies.

Study	Source or Environment	Particle size range (nm)	Instrument	N × 10^{15} (kg-fuel^{-1})
This work	Solid and gas fuel cookstoves	1.1–1000	A11-nCNC	10–40
Shen et al. (2017)	Solid fuel cookstoves	14.6–661	SMPS	1–7
Bilsback et al. (2019)	Solid fuel cookstoves	10–100	SMPS	0.4–16
	Gas fuel cookstoves	10–100	SMPS	0.1–7
Alanen et al. (2015)#	Natural gas engine	1.7–1000	A11-nCNC	0.1–1
Pirjola et al. (2016)	Diesel, ethanol, CNG buses	5.6–560	EEPS&	0.03–2
Giechaskiel et al. (2017)*	Gasoline vehicles	5.6–560	EEPS&	0.004–0.03
	Diesel vehicles		EEPS&	0.0003–0.001
	2-/4-stroke mopeds		EEPS&	0.02–0.2
Rönkkö et al. (2017)	Diesel engine	1.3–1000	A11-nCNC	0.001–4.3
Järvinen et al. (2019)	Diesel buses	1.3–1000	A11-nCNC	0.2–2
Rönkkö et al. (2017)	Traffic and street canyon	1.3–1000	A11-nCNC	2.5
Hietikko et al. (2018)	Street canyon	1–1000	A11-nCNC	5

#Assuming a fuel consumption of 0.2 kg kWh^{-1}.
*Assuming a fuel economy of 30 miles gallon^{-1} or 12 km L^{-1}.
&EEPS = engine exhaust particle sizer (TSI Inc.).

were much higher on account of the smallest size measured by those two other studies. Our N_1 emissions were generally much larger (factors of 1–10^4) than those measured in the tailpipe exhaust of internal combustion engines (Järvinen et al. 2019; Giechaskiel et al. 2017; Rönkkö et al. 2017; Pirjola et al. 2016; Alanen et al. 2015) and in near-road environments (Hietikko et al. 2018; Rönkkö et al. 2017). The N_1 emissions from the cookstoves approached those measured in the other studies when the emissions were sampled from high emitters (e.g., 2-stroke moped in Giechaskiel et al. (2017)), when the engines were operated at higher loads (e.g., modern diesel engine in Rönkkö et al. (2017)), or in peak traffic conditions (Rönkkö et al. 2017). These results suggest that cookstoves, on an emission factor basis, might be a much larger source of sub-10 nm particle emissions to the atmosphere than traffic-related sources.

We compared median particle size distributions gathered from the A11 and SMPS on an emission factor basis in Figure 3 for all five cookstoves; averaged particle size distributions along with the standard deviation are shown in Figure S4. All cookstoves, including LPG, produced high particle number emissions in the size range of 1.1 to 3 nm and these emissions were largely consistent between the different cookstoves. The sub 5-nm particles had a distinct mode separate from the larger modes seen at particle sizes above 10 nm. These observations were used to inform particle emissions and the initial size distribution for the sub-10 nm mode in GEOS-Chem-TOMAS (details in Section 3.3).

3.3. Geos-Chem-TOMAS simulation results

Earlier measurements and those performed in this work were used to inform the inclusion of sub-10 nm particles into GEOS-Chem-TOMAS for all anthropogenic combustion sources (e.g., fossil fuels, biofuels). Sub-10 nm particles were not added for natural

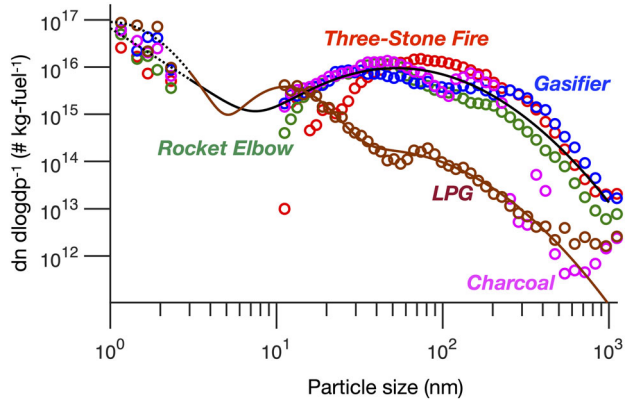

Figure 3. Median size distributions for particle emissions from the five different cookstoves based on data from the A11 and SMPS instruments. The solid lines are log-normal fits to the data to guide the eye. We used a bimodal fit for the solid fuel cookstoves (solid black) and a trimodal fit for the LPG (solid brown). The solid lines were used to inform the particle size distributions in GEOS-Chem-TOMAS.

combustion emissions sources (e.g., biomass burning) although it is likely that biomass burning, similar to cookstoves, may contribute to emissions of sub-10 nm particles. The median sub-10 nm particle number emissions were found to be 43% to 96% of the total particle number emissions across the five different cookstoves (see Figure 2c). This meant that the number emissions of sub-10 nm particles were, on median, a factor of 0.75 to 24 higher than the super-10 nm particles. Sub-10 nm particle number emissions from mobile sources in laboratory studies and in near-road environments have also been found to be slightly less than or equal to the number emissions of super-10 nm particles (Giechaskiel et al. 2017; Rönkkö et al. 2017). Based on these observations, the initial number of sub-10 nm particle emissions in GEOS-Chem-TOMAS were determined by scaling the number emissions for the larger mode (μ=60 nm, $\sigma = 2$) by a factor of 1 and 10. The factors of 1 and 10 were chosen for simplicity and to illustrate the approximate sensitivity in model predictions to addition of sub-10 nm particles. The distribution of particles in diameters below 10 nm was determined by fitting a bimodal log-normal distribution to the median particle size distribution measured for the solid fuel cookstoves (see Figure 3). The smaller mode had a μ of 1 nm and a σ of 2. As the smallest size tracked in GEOS-Chem-TOMAS is 3 nm, we only modeled the size distribution for the particle sizes larger than 3 nm. By doing so, we assumed that all particles in the smaller mode had survived to sizes larger than 3 nm while maintaining the shape of the size distribution to be injected into the GEOS-Chem-TOMAS grid cell. In our simulation all emissions, including anthropogenic combustion, were instantly mixed into the 4° x 5° grid cells upon emission, assuming that these emissions were not affected by additional sub-grid scale processes (e.g., coagulation in plumes). Thus, the results from our simulations represent an upper bound of the effects of sub-10 nm particles on particle number concentrations and the cloud-albedo indirect effect.

Annually averaged changes in the particle number concentrations at the surface and the cloud-albedo indirect effect from the GEOS-Chem simulations for the year 2016 are presented in Figure 4. These results represent the percent changes simulated between the SUB10_1× and BASE simulations, i.e., SUB10_1×-BASE. A 1-fold addition of sub-10 nm particle emissions from anthropogenic combustion sources resulted in a globally averaged increase of 20% (range: −20% to + 2,500%) in the surface concentrations of sub-10 nm particles. We found the largest increases in sub-10 nm particle concentrations in the tropics where biofuel combustion is still an important source for cooking and heating needs. The increases in the temperate zone were relatively minor (<1%), and it is possible that in these regions the emissions of sub-10 nm particles from combustion sources were competing with the nucleation rate that dominates particle number concentrations below 10 nm (Westervelt, Pierce, and Adams 2014). The 1-fold addition of sub-10 nm particle emissions had a much smaller effect on particles larger than 10 nm. The simulations produced a globally averaged increase of 0.02% (range: −2% to +3%) and 0.01% (range: −1% to +1%) in the surface concentrations of super-10 nm particles and CCN-relevant sizes (>80 nm) (Figure 4b–c), respectively. Mirroring the increases, there were also regions where there were decreases in the number concentrations of sub-10, super-10 nm, and CCN-relevant particles. These are likely to be from small increases in the condensational sink in the source and outflow regions that dampened nucleation rates. A 10-fold addition of sub-10 nm particle emissions produced a stronger increase in the surface concentrations of sub-10 nm particles (globally averaged increase of 200% with a range of -20% to +2,500%) but still produced relatively small increases in surface concentrations of super-10 nm (globally averaged increase of 0.16% with a range of -2% to +10%) and CCN-relevant particles (globally averaged increase of 0.09% with a range of -1% to +6%). The results for SUB10_10×-BASE are presented in Figure S5.

Finally, the simulations produced a negligible change in the cloud-albedo indirect effect with the strongest localized effects ranging from -0.2 W m^{-2} to

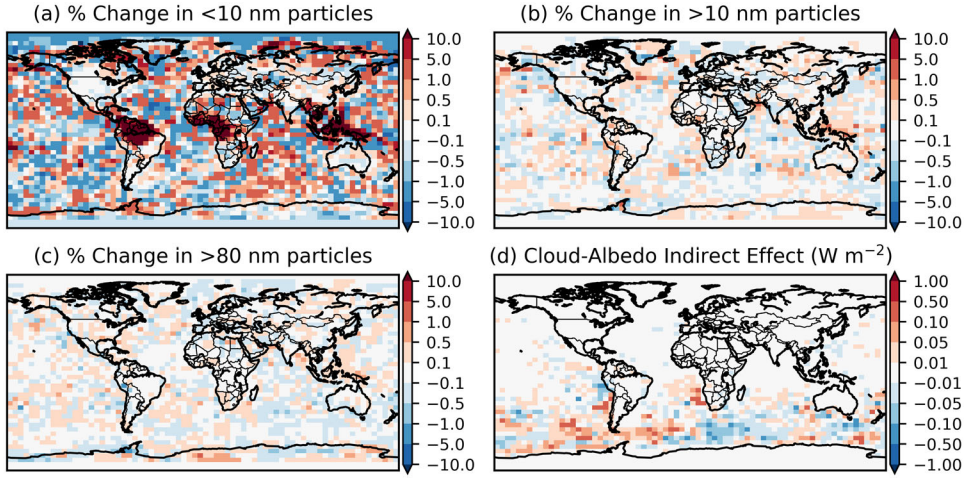

Figure 4. Annually averaged change in (a) <10 nm, (b) >10 nm, and (c) >80 nm particle number concentrations after a 1-fold addition of sub-10 nm particles from anthropogenic combustion sources to GEOS-Chem (SUB10_1×-BASE). (d) Annually averaged cloud-albedo indirect effect associated with the addition of sub-10 nm particles from all anthropogenic combustion sources (i.e., excluding biomass burning).

+0.2 W m^{-2} and globally averaged values of +0.001 W m^{-2}. Positive values of the cloud-albedo indirect effect indicate that the addition of sub-10 nm particles produced a net warming while negative values indicate that those particles produced a net cooling. For reference, the global mean aerosol indirect effect that includes the cloud-albedo indirect effect is -0.55 (-0.06 to -1.33 W m^{-2}) (IPCC. 2014). Over land the largest impacts, which were still relatively minor (<0.05 W m^{-2}), were seen in Brazil, southern Africa, and parts of southeast Asia, all regions with heavy biofuel combustion. Although the signal was noisy, the strongest cloud-albedo indirect effect was seen over the Southern Ocean. This was because the region has lower background particle number concentrations and more liquid-phase clouds, both of which make the region more susceptible to changes in CCN (Hodshire et al. 2019).

The two sensitivity simulations (SUB10_1×$_{mod}$, SUB10_10×$_{mod}$) that used a different log-normal distribution (μ of 30 nm and σ of 2) to represent the larger mode produced a slightly higher increase in sub- and super-10 nm particle concentrations at the surface when compared to the BASE$_{mod}$ simulation, which also used a μ of 30 nm and σ of 2 for the larger mode (Figures S6 and S7 respectively). The globally averaged increases in sub-10, super-10, and CCN-relevant (>80 nm) sizes were 68%, 0.55%, and 0.23%, respectively, for the SUB10_1×$_{mod}$ simulation and 640%, 4.6%, and 1.7%, respectively, for the SUB10_10×$_{mod}$ simulation. With little change in globally averaged CCN-relevant sizes (0.23% and 1.7%), the globally averaged cloud-albedo indirect effect was -0.004 and -0.038 W m^{-2} for the SUB10_1×$_{mod}$ and SUB10_10×$_{mod}$ simulations, respectively.

4. Summary and discussion

In this work, we measured number emissions of particles ranging in diameter from ~1 to ~1000 nm for five different cookstoves. The combustion sources studied include traditional, improved, and gas fueled cookstoves: three-stone fire, rocket elbow, gasifier, charcoal, and LPG. As expected, the number emissions for particles with diameters larger than 10 nm were an order of magnitude lower for the gas fuel cookstove (i.e., LPG) than the solid fuel cookstoves. But both solid and gas (i.e., LPG) fuel cookstoves produced similar and significant number emissions for particles with diameters below 10 nm (>5 × 10^{15} # kg-$fuel^{-1}$). These emissions of sub-10 nm particles accounted for nearly half (for the three-stone fire) to more than 90% (for the LPG) of the total particle number emissions above ~1 nm. For the cookstoves studied in this work, the total and sub-10 nm particle number emissions were significantly larger than those measured earlier from mobile sources (Järvinen et al. 2019; Rönkkö et al. 2017; Alanen et al. 2015). The addition of the sub-10 nm particle emissions to a global chemical transport model substantially increased surface concentrations of sub-10 nm particles (20-70%, globally averaged) but had little influence on globally averaged CCN-relevant sizes (0.01-0.23%) or the cloud-albedo indirect effect (-0.004-0.001 W m^{-2}). Overall, we find that biofuel combustion is a large primary source of sub-10 nm particles to the atmosphere, but it is unlikely that the sub-10 nm particle emissions will have any measurable radiative effects. Regardless, we urge continued study of the emissions, evolution, composition, and properties of sub-10 nm particles from combustion and energy sources.

We did not measure the chemical composition of the sub-10 nm particles emitted by the cookstoves but, based on earlier work done on internal combustion engines, these particles are likely to be composed of sulfuric acid and/or low-volatility organic compounds that nucleate and grow as the combustion exhaust from the cookstove is diluted and cooled in the emissions hood (Alanen et al. 2015; Rönkkö et al. 2007; Kittelson, Watts, and Johnson 2006). In this work, the emissions hood used in this study diluted the emissions from the cookstove with particle-laden background air and the diluted emissions had a residence time of slightly under a minute before they were sampled. We found that the sub-10 nm particles were formed throughout the water boiling test and were formed for all cookstoves, suggesting that the conditions (e.g., dilution, mixing, emissions of low-volatility compounds, condensational sink of the nonvolatile fraction) were always conducive for the formation of these sub-10 nm particles. This may not always be the case. For example, diesel exhaust diluted with clean air in a dilution tunnel leads to new particle formation and significant increases in measured particle number emissions only under the right input (e.g., high sulfur content in the fuel), operating (e.g., high relative humidity), and load (e.g., idling) conditions (Abdul-Khalek, Kittelson, and Brear 1999). Without a fundamental understanding of the chemical constituents and the physical processes that lead to new particle formation and growth, it is unclear if the conditions simulated in the emissions hood in this work are representative of those in the real world. We propose that future work measure emissions of sub-10 nm particles from biofuel combustion in field environments.

Coagulation lifetimes for sub-10 nm particles are known to be short. At a $PM_{2.5}$ mass concentration of 50 μg m^{-3} characteristic of the most polluted countries that have significant biofuel use (van Donkelaar et al. 2010) and an urban aerosol size distribution, coagulation e-folding lifetimes range from a few seconds to a few minutes for 1–10 nm particles (Pandis and Seinfeld 2006). This would change to 1–20 min, respectively, at a $PM_{2.5}$ mass concentration of 5 μg m^{-3} but will remain unchanged for particle size distributions representative of rural or remote continental backgrounds. This rapid loss of sub-10 nm particles to coagulation, which was simulated in GEOS-Chem-TOMAS, is probably the primary reason why a 1- and 10-fold addition of these particles had little impact on concentrations of CCN-relevant sizes and the aerosol indirect effect. However, we did not account for coagulation in exhaust plumes where the number and mass concentrations would be significantly higher than the grid cell-level concentrations simulated in GEOS-Chem-TOMAS. If accounted for, this would tend to further accelerate the loss of sub-10 nm particles and even further dampen their influence on ambient concentrations and climate impacts.

Combustion sources are known to be important contributors to ultrafine particles (UFPs) (Hu et al. 2017) – defined as particles smaller than 100 nm – in the atmosphere although this finding is largely based on measurements and modeling performed on particle diameters larger than 10 nm. This work indicates that fossil fuel and biofuel combustion sources may also contribute substantially to the UFP burden through emissions of sub-10 nm particles. Exposure to UFPs has been postulated to be as or more important than $PM_{2.5}$ for human health (Ostro et al. 2015; Hoek et al. 2010) although UFPs are not routinely measured to the same extent as $PM_{2.5}$ and, hence, their concentrations, composition, spatiotemporal distribution, and potential health impacts remain largely uncertain. For instance, in addition to their potential to deposit in the pulmonary region of the respiratory system and cross the air-blood barrier, particles smaller than 50 nm can also deposit in the extrathoracic region (i.e., head airways) and translocate to the brain and affect the central nervous system (Kao et al. 2012). So while sub-10 nm particle emissions from combustion sources may not have substantial radiative effects, they need to be studied further for their impacts on human health, especially in near-source environments.

Contributions

SHJ and NS designed the research. NS conducted the cookstove experiments. SHJ and NS analyzed the data. KB and JRP configured the inputs for GEOS-Chem and KB performed the simulations and analyzed the GEOS-Chem data. TDG and JV (Airmodus) facilitated access to the A11 nCNC instrument and JV (CSU) facilitated access to the SMPS.

Data sharing

The data presented in the figures in the main text can be found at the following archival link: http://dx.doi.org/10.25675/10217/207240. For data presented in the supplemental material, please contact the corresponding author.

Funding

This work was partly supported by the National Oceanic and Atmospheric Administration (NA17OAR4310003 and NA17OAR4310001) and the National Science Foundation

(HCBU AGS-1831013). We thank Airmodus Inc. (Finland) for providing access and technical support for the A11 nCNC system. We also thank Kirk Evans and John Mizia from the Energy Institute for support with the cookstove experiments.

ORCID

John Volckens http://orcid.org/0000-0002-7563-9525

References

Abdul-Khalek, I., D. Kittelson, and F. Brear. 1999. The influence of dilution conditions on diesel exhaust particle size distribution measurements. *SAE Trans. J. Mater. Manuf.* 108:563–71.

Abdul-Razzak, H., and S. J. Ghan. 2002. A parameterization of aerosol activation 3. Sectional representation. *J. Geophys. Res.* 107 (D3):4026.

Adams, P. J., and J. H. Seinfeld. 2002. Predicting global aerosol size distributions in general circulation models. *J. Geophys. Res.* 107 (D19):13,791. doi:10.1029/2001JD001010.

Adams, P. J., J. H. Seinfeld, D. Koch, L. Mickley, and D. Jacob. 2001. General circulation model assessment of direct radiative forcing by the sulfate-nitrate-ammonium-water inorganic aerosol system. *J. Geophys. Res.* 106 (D1): 1097–111. doi:10.1029/2000JD900512.

Alanen, J., E. Saukko, K. Lehtoranta, T. Murtonen, H. Timonen, R. Hillamo, P. Karjalainen, H. Kuuluvainen, J. Harra, J. Keskinen, et al. 2015. The formation and physical properties of the particle emissions from a natural gas engine. *Fuel* 162:155–61. doi:10.1016/j.fuel.2015.09.003.

Albalak, R., N. Bruce, J. P. McCracken, K. R. Smith, and T. De Gallardo. 2001. Indoor respirable particulate matter concentrations from an open fire, improved cookstove, and LPG/open fire combination in a rural Guatemalan community. *Environ. Sci. Technol.* 35 (13):2650–5. doi:10.1021/es001940m.

Apte, J. S., J. D. Marshall, A. J. Cohen, and M. Brauer. 2015. Addressing global mortality from ambient PM2.5. *Environ. Sci. Technol.* 49 (13):8057–66. doi:10.1021/acs.est.5b01236.

Bilsback, K. R., J. Dahlke, K. M. Fedak, N. Good, A. Hecobian, P. Herckes, C. L'Orange, J. Mehaffy, A. Sullivan, J. Tryner, et al. 2019. A laboratory assessment of 120 air pollutant emissions from biomass and fossil fuel cookstoves. *Environ. Sci. Technol.* 53 (12):7114–25. doi:10.1021/acs.est.8b07019.

Carnerero, C., N. Perez, C. Reche, M. Ealo, G. Titos, H.-K. Lee, H.-R. Eun, Y.-H. Park, L. Dada, P. Paasonen, et al. 2018. Vertical and horizontal distribution of regional new particle formation events in Madrid. *Atmos. Chem. Phys.* 18 (22):16601–18. doi:10.5194/acp-18-16601-2018.

Clark, M. L., S. J. Reynolds, J. B. Burch, S. Conway, A. M. Bachand, and J. L. Peel. 2010. Indoor air pollution, cookstove quality, and housing characteristics in two Honduran communities. *Environ. Res.* 110 (1):12–8. doi:10.1016/j.envres.2009.10.008.

D'Andrea, S. D., S. A. K. Häkkinen, D. M. Westervelt, C. Kuang, E. J. T. Levin, V. P. Kanawade, W. R. Leaitch, D. V. Spracklen, I. Riipinen, and J. R. Pierce. 2013. Understanding global secondary organic aerosol amount and size-resolved condensational behavior. *Atmos. Chem. Phys.* 13 (22):11519–34. doi:10.5194/acp-13-11519-2013.

Fuzzi, S., U. Baltensperger, K. Carslaw, S. Decesari, H. Denier van der Gon, M. C. Facchini, D. Fowler, I. Koren, B. Langford, U. Lohmann, et al. 2015. Particulate matter, air quality and climate: Lessons learned and future needs. *Atmos. Chem. Phys.* 15 (14):8217–99. doi:10.5194/acp-15-8217-2015.

Giechaskiel, B., J. Vanhanen, M. Väkevä, and G. Martini. 2017. Investigation of vehicle exhaust sub-23 nm particle emissions. *Aerosol Sci. Technol* 51 (5):626–41. doi:10.1080/02786826.2017.1286291.

Gordon, H., J. Kirkby, U. Baltensperger, F. Bianchi, M. Breitenlechner, J. Curtius, A. Dias, J. Dommen, N. M. Donahue, E. M. Dunne, et al. 2017. Causes and importance of new particle formation in the present-day and preindustrial atmospheres. *J. Geophys. Res. Atmos.* 122 (16):8739–60. doi:10.1002/2017JD026844.

Granier, C., B. Bessagnet, T. Bond, A. D'Angiola, H. Denier van der Gon, G. J. Frost, A. Heil, J. W. Kaiser, S. Kinne, Z. Klimont, et al. 2011. Evolution of anthropogenic and biomass burning emissions of air pollutants at global and regional scales during the 1980–2010 period. *Clim. Change* 109 (1-2):163–90. doi:10.1007/s10584-011-0154-1.

Guenther, A. B., X. Jiang, C. L. Heald, T. Sakulyanontvittaya, T. Duhl, L. K. Emmons, and X. Wang. 2012. The Model of Emissions of Gases and Aerosols from Nature version 2.1 (MEGAN2.1): An extended and updated framework for modeling biogenic emissions. *Geosci. Model Dev.* 5 (6):1471–92. doi:10.5194/gmd-5-1471-2012.

Herner, J. D., S. Hu, W. H. Robertson, T. Huai, M.-C. O. Chang, P. Rieger, and A. Ayala. 2011. Effect of advanced aftertreatment for PM and NOx reduction on heavy-duty diesel engine ultrafine particle emissions. *Environ. Sci. Technol.* 45 (6):2413–9. doi:10.1021/es102792y.

Hietikko, R., H. Kuuluvainen, R. M. Harrison, H. Portin, H. Timonen, J. V. Niemi, and T. Rönkkö. 2018. Diurnal variation of nanocluster aerosol concentrations and emission factors in a street canyon. *Atmos. Environ.* 189: 98–106. doi:10.1016/j.atmosenv.2018.06.031.

Hinds, W. C. 2012. *Aerosol technology: Properties, behavior, and measurement of airborne particles*. Hoboken, NJ: John Wiley & Sons.

Hodshire, A. L., P. Campuzano-Jost, J. K. Kodros, B. Croft, B. A. Nault, J. C. Schroder, J. L. Jimenez, and J. R. Pierce. 2019. The potential role of methanesulfonic acid (MSA) in aerosol formation and growth and the associated radiative forcings. *Atmos. Chem. Phys.* 19 (5): 3137–60. doi:10.5194/acp-19-3137-2019.

Hoek, G., H. Boogaard, A. Knol, J. de Hartog, P. Slottje, J. G. Ayres, P. Borm, B. Brunekreef, K. Donaldson, F. Forastiere, et al. 2010. Concentration response functions for ultrafine particles and all-cause mortality and hospital admissions: Results of a European expert panel elicitation. *Environ. Sci. Technol.* 44 (1):476–82. doi:10.1021/es9021393.

Hoesly, R. M., S. J. Smith, L. Feng, Z. Klimont, G. Janssens-Maenhout, T. Pitkanen, J. J. Seibert, L. Vu, R. J. Andres, R. M. Bolt, et al. 2018. Historical (1750–2014) anthropogenic emissions of reactive gases and aerosols from the Community Emission Data System (CEDS). *Geosci. Model Dev.* 11 (1):369–408. doi:10.5194/gmd-11-369-2018.

Hu, J., S. Jathar, H. Zhang, Q. Ying, S. Chen, C. Cappa, and M. Kleeman. 2017. Long-term particulate matter modeling for health effect studies in California–Part 2: Concentrations and sources of ultrafine organic aerosols. *Atmos. Chem. Phys.* 17 (8):5379–91. doi:10.5194/acp-17-5379-2017.

Huang, C., D. Lou, Z. Hu, Q. Feng, Y. Chen, C. Chen, P. Tan, and D. Yao. 2013. A PEMS study of the emissions of gaseous pollutants and ultrafine particles from gasoline- and diesel-fueled vehicles. *Atmos. Environ.* 77: 703–10. doi:10.1016/j.atmosenv.2013.05.059.

Iacono, M. J., J. S. Delamere, E. J. Mlawer, M. W. Shephard, S. A. Clough, and W. D. Collins. 2008. Radiative forcing by long-lived greenhouse gases: Calculations with the AER radiative transfer models. *J. Geophys. Res.* 113 (D13):D13103. doi:10.1029/2008JD009944.

IPCC. 2014. Climate change 2014: Synthesis report. Contribution of Working Groups I, II and III to the Fifth Assessment Report of the Intergovernmental Panel on Climate Change. Geneva, Switzerland: IPCC, 151 pp.

Jaeglé, L., P. K. Quinn, T. S. Bates, B. Alexander, and J.-T. Lin. 2011. Global distribution of sea salt aerosols: New constraints from in situ and remote sensing observations. *Atmos. Chem. Phys.* 11 (7):3137–57. doi:10.5194/acp-11-3137-2011.

Järvinen, A., H. Timonen, P. Karjalainen, M. Bloss, P. Simonen, S. Saarikoski, H. Kuuluvainen, J. Kalliokoski, M. Dal Maso, J. V. Niemi, et al. 2019. Particle emissions of Euro VI, EEV and retrofitted EEV city buses in real traffic. *Environ. Pollut.* 250:708–16. doi:10.1016/j.envpol.2019.04.033.

Jetter, J., Y. Zhao, K. R. Smith, B. Khan, T. Yelverton, P. DeCarlo, and M. Hays. 2012. Pollutant emissions and energy efficiency under controlled conditions for household biomass cookstoves and implications for metrics useful in setting international test standards. *Environ. Sci. Technol.* 46 (19):10827–34. doi:10.1021/es301693f.

Jung, J., B. Tsatsral, Y. J. Kim, and K. Kawamura. 2010. Organic and inorganic aerosol compositions in Ulaanbaatar, Mongolia, during the cold winter of 2007 to 2008: Dicarboxylic acids, ketocarboxylic acids, and α-dicarbonyls. *J. Geophys. Res.* 115 (D22):D22203. doi:10.1029/2010JD014339.

Just, B., S. Rogak, and M. Kandlikar. 2013. Characterization of ultrafine particulate matter from traditional and improved biomass cookstoves. *Environ. Sci. Technol.* 47 (7):3506–12. doi:10.1021/es304351p.

Kangasluoma, J., A. Franchin, J. Duplissy, L. Ahonen, F. Korhonen, M. Attoui, J. Mikkilä, K. Lehtipalo, J. Vanhanen, M. Kulmala, et al. 2016. Operation of the Airmodus A11 nano Condensation Nucleus Counter at various inlet pressures and various operation temperatures, and design of a new inlet system. *Atmos. Meas. Tech.* 9 (7):2977–88. doi:10.5194/amt-9-2977-2016.

Kao, Y.-Y., T.-J. Cheng, D.-M. Yang, C.-T. Wang, Y.-M. Chiung, and P.-S. Liu. 2012. Demonstration of an olfactory bulb-brain translocation pathway for ZnO nanoparticles in rodent cells in vitro and in vivo. *J. Mol. Neurosci.* 48 (2):464–71. doi:10.1007/s12031-012-9756-y.

Kerminen, V.-M., and A. S. Wexler. 1996. The occurrence of sulfuric acid-water nucleation in plumes: Urban environment. *Tellus B Chem. Phys. Meteorol.* 48 (1):65–82. doi:10.1034/j.1600-0889.1996.00007.x.

Kittelson, D. B., W. F. Watts, and J. P. Johnson. 2006. On-road and laboratory evaluation of combustion aerosols—Part1: Summary of diesel engine results. *J. Aerosol Sci* 37 (8):913–30. doi:10.1016/j.jaerosci.2005.08.005.

Kodros, J. K., C. E. Scott, S. C. Farina, Y. H. Lee, C. L&Apos;Orange, J. Volckens, and J. R. Pierce. 2015. Uncertainties in global aerosols and climate effects due to biofuel emissions. *Atmos. Chem. Phys.* 15 (15):8577–96. doi:10.5194/acp-15-8577-2015.

Kodros, J. K., C. Wiedinmyer, B. Ford, R. Cucinotta, R. Gan, S. Magzamen, and J. R. Pierce. 2016. Global burden of mortalities due to chronic exposure to ambient PM2. 5 from open combustion of domestic waste. *Environ. Res. Lett.* 11 (12):124022. doi:10.1088/1748-9326/11/12/124022.

Kuang, C., P. H. McMurry, and A. V. McCormick. 2009. Determination of cloud condensation nuclei production from measured new particle formation events. *Geophys. Res. Lett.* 36 (9):1227. doi:10.1029/2009GL037584.

Lee, S. S., and G. Feingold. 2013. Aerosol effects on the cloud-field properties of tropical convective clouds. *Atmos. Chem. Phys.* 13 (14):6713–26. doi:10.5194/acp-13-6713-2013.

Li, M., Q. Zhang, J.-I. Kurokawa, J.-H. Woo, K. He, Z. Lu, T. Ohara, Y. Song, D. G. Streets, G. R. Carmichael, et al. 2017. MIX: A mosaic Asian anthropogenic emission inventory under the international collaboration framework of the MICS-Asia and HTAP. *Atmos. Chem. Phys.* 17 (2):935–63. doi:10.5194/acp-17-935-2017.

Marais, E. A., and C. Wiedinmyer. 2016. Air Quality Impact of Diffuse and Inefficient Combustion Emissions in Africa (DICE-Africa). *Environ. Sci. Technol.* 50 (19): 10739–45. doi:10.1021/acs.est.6b02602.

Ostro, B., J. Hu, D. Goldberg, P. Reynolds, A. Hertz, L. Bernstein, and M. J. Kleeman. 2015. Associations of mortality with long-term exposures to fine and ultrafine particles, species and sources: Results from the California Teachers Study Cohort. *Environ. Health Perspect.* 123 (6): 549–56. doi:10.1289/ehp.1408565.

Pachauri, R. K., M. R. Allen, V. R. Barros, J. Broome, W. Cramer, R. Christ, J. A. Church, L. Clarke, Q. Dahe, P. Dasgupta, et al. 2014. Climate Change 2014: Synthesis Report. Contribution of Working Groups I, II and III to the Fifth Assessment Report of the Intergovernmental Panel on Climate Change. IPCC, Geneva, Switzerland.

Pai, S. J., C. L. Heald, J. R. Pierce, S. C. Farina, E. A. Marais, J. L. Jimenez, P. C. Jost, B. A. Nault, A. M. Middlebrook, H. Coe, et al. 2020. An evaluation of global organic aerosol schemes using airborne observations. *Atmos. Chem. Phys.* 20 (5):2637–65. doi:10.5194/acp-20-2637-2020.

Pandis, S. N., and J. H. Seinfeld. 2006. *Atmospheric chemistry and physics: From air pollution to climate change.* Hoboken, NJ: Wiley.

Park, E., and K. Lee. 2003. Particulate exposure and size distribution from wood burning stoves in Costa Rica. *Indoor Air.* 13 (3):253–9. doi:10.1034/j.1600-0668.2003.00194.x.

Petters, M. D., and S. M. Kreidenweis. 2007. A single parameter representation of hygroscopic growth and cloud condensation nucleus activity. *Atmos. Chem. Phys.* 7 (8): 19661–1971.

Pierce, J. R., K. Chen, and P. J. Adams. 2007. Contribution of primary carbonaceous aerosol to cloud condensation nuclei: Processes and uncertainties evaluated with a global aerosol microphysics model. *Atmos. Chem. Phys.* 7 (20):5447–66. doi:10.5194/acp-7-5447-2007.

Pierce, J. R., I. Riipinen, M. Kulmala, M. Ehn, T. Petaja, H. Junninen, D. R. Worsnop, and N. M. Donahue. 2011. Quantification of the volatility of secondary organic compounds in ultrafine particles during nucleation events. *Atmos. Chem. Phys.* 11 (17):9019–36. doi:10.5194/acp-11-9019-2011.

Pirjola, L., A. Dittrich, J. V. Niemi, S. Saarikoski, H. Timonen, H. Kuuluvainen, A. Järvinen, A. Kousa, T. Rönkkö, and R. Hillamo. 2016. Physical and chemical characterization of real-world particle number and mass emissions from city buses in Finland. *Environ. Sci. Technol.* 50 (1):294–304. doi:10.1021/acs.est.5b04105.

Raiyani, C. V., S. H. Shah, N. M. Desai, K. Venkaiah, J. S. Patel, D. J. Parikh, and S. K. Kashyap. 1993. Characterization and problems of indoor pollution due to cooking stove smoke. *Atmos. Environ. Part A* 27 (11): 1643–55. doi:10.1016/0960-1686(93)90227-P.

Ramnarine, E., J. K. Kodros, A. L. Hodshire, C. R. Lonsdale, M. J. Alvarado, and J. R. Pierce. 2019. Effects of near-source coagulation of biomass burning aerosols on global predictions of aerosol size distributions and implications for aerosol radiative effects. *Atmos. Chem. Phys.* 19 (9): 6561–77. doi:10.5194/acp-19-6561-2019.

Rap, A., C. E. Scott, D. V. Spracklen, N. Bellouin, P. M. Forster, K. S. Carslaw, A. Schmidt, and G. Mann. 2013. Natural aerosol direct and indirect radiative effects. *Geophys. Res. Lett.* 40 (12):3297–301. doi:10.1002/grl.50441.

Rönkkö, T., H. Kuuluvainen, P. Karjalainen, J. Keskinen, R. Hillamo, J. V. Niemi, L. Pirjola, H. J. Timonen, S. Saarikoski, E. Saukko, et al. 2017. Traffic is a major source of atmospheric nanocluster aerosol. *Proc. Natl. Acad. Sci. USA.* 114 (29):7549–54. doi:10.1073/pnas.1700830114.

Rönkkö, T., A. Virtanen, J. Kannosto, J. Keskinen, M. Lappi, and L. Pirjola. 2007. Nucleation mode particles with a nonvolatile core in the exhaust of a heavy duty diesel vehicle. *Environ. Sci. Technol.* 41 (18):6384–9. doi:10.1021/es0705339.

Scott, W. T. 1968. Analytic studies of cloud droplet coalescence I. *J. Atmos. Sci.* 25 (1):54–65. doi:10.1175/1520-0469(1968)025<0054:ASOCDC>2.0.CO;2.

Shen, G., C. K. Gaddam, S. M. Ebersviller, R. L. Vander Wal, C. Williams, J. W. Faircloth, J. J. Jetter, and M. D. Hays. 2017. A laboratory comparison of emission factors, number size distributions, and morphology of ultrafine particles from 11 different household cookstove-fuel systems. *Environ. Sci. Technol.* 51 (11):6522–32. doi:10.1021/acs.est.6b05928.

Spracklen, D. S., K. S. Carslaw, M. Kulmala, V.-M. Kerminen, S.-L. Sihto, and I. Riipinen. 2007. The Impact of boundary layer nucleation on global CCN. In *Nucleation and Atmospheric Aerosols*, ed. C. D. O'Dowd and P. E. Wagner, 911–5. Dordrecht, Netherlands: Springer.

Spracklen, D., K. Carslaw, U. Pöschl, A. Rap, and P. M. Forster. 2011. Global cloud condensation nuclei influenced by carbonaceous combustion aerosol. *Atmos. Chem. Phys.* 11 (17):9067–87. doi:10.5194/acp-11-9067-2011.

Stevens, R. G., J. R. Pierce, C. A. Brock, M. K. Reed, J. H. Crawford, J. S. Holloway, T. B. Ryerson, L. G. Huey, and J. B. Nowak. 2012. Nucleation and growth of sulfate aerosol in coal-fired power plant plumes: Sensitivity to background aerosol and meteorology. *Atmos. Chem. Phys.* 12 (1):189–206. doi:10.5194/acp-12-189-2012.

Stolzenburg, M. R., J. H. T. Scheckman, M. Attoui, H.-S. Han, and P. H. McMurry. 2018. Characterization of the TSI model 3086 differential mobility analyzer for classifying aerosols down to 1 nm. *Aerosol Sci. Technol.* 52 (7): 748–56. doi:10.1080/02786826.2018.1456649.

Tryner, J., J. W. Tillotson, M. E. Baumgardner, J. T. Mohr, M. W. DeFoort, and A. J. Marchese. 2016. The effects of air flow rates, secondary air inlet geometry, fuel type, and operating mode on the performance of gasifier cookstoves. *Environ. Sci. Technol.* 50 (17):9754–63. doi:10.1021/acs.est.6b00440.

Tryner, J., J. Volckens, and A. J. Marchese. 2018. Effects of operational mode on particle size and number emissions from a biomass gasifier cookstove. *Aerosol Sci. Technol.* 52 (1):87–97. doi:10.1080/02786826.2017.1380779.

van der Werf, G. R., J. T. Randerson, L. Giglio, T. T. van Leeuwen, Y. Chen, B. M. Rogers, M. Mu, M. J. E. van Marle, D. C. Morton, G. J. Collatz, et al. 2017. Global fire emissions estimates during 1997-2016. *Earth Syst. Sci. Data* 9 (2):697–720. doi:10.5194/essd-9-697-2017.

van Donkelaar, A., R. V. Martin, M. Brauer, R. Kahn, R. Levy, C. Verduzco, and P. J. Villeneuve. 2010. Global estimates of ambient fine particulate matter concentrations from satellite-based aerosol optical depth: Development and application. *Environ. Health Perspect.* 118 (6):847–55. doi:10.1289/ehp.0901623.

Von der Weiden, S. L., F. Drewnick, and S. Borrmann. 2009. Particle Loss Calculator–a new software tool for the assessment of the performance of aerosol inlet systems. *Atmos. Meas. Tech.* 2 (2):479–94. doi:10.5194/amt-2-479-2009.

Ward, D. E. 1990. Factors influencing the emissions of gases and particulate matter from biomass burning. In *Fire in the tropical biota: Ecosystem processes and global challenges*, ed. J. G. Goldammer, 418–36. Berlin, Heidelberg: Springer Berlin Heidelberg.

WBT (Water Boiling Test). 2014. Version 4.2.3. //www.cleancookingalliance.org/binary-data/DOCUMENT/file/000/000/399-1.pdf

Westervelt, D. M., J. R. Pierce, and P. J. Adams. 2014. Analysis of feedbacks between nucleation rate, survival probability and cloud condensation nuclei formation. *Atmos. Chem. Phys.* 14 (11):5577–97. doi:10.5194/acp-14-5577-2014.

Westervelt, D. M., J. R. Pierce, I. Riipinen, W. Trivitayanurak, A. Hamed, M. Kulmala, A. Laaksonen, S.

Decesari, and P. J. Adams. 2013. Formation and growth of nucleated particles into cloud condensation nuclei: Model-measurement comparison. *Atmos. Chem. Phys.* 13 (15):7645–63. doi:10.5194/acp-13-7645-2013.

Zender, C. S. 2003. Mineral Dust Entrainment and Deposition (DEAD) model: Description and 1990s dust climatology. *J. Geophys. Res.* 108 (D14):18,075. doi:10.1029/2002JD002775.